

Quantum electronic transport of topological surface states in β -Ag₂Se nanowire

Jihwan Kim,^{1,†} Ahreum Hwang,^{1,†} Sang-Hoon Lee,² Seung-Hoon Jhi,² Sunghun Lee,¹ Yun Chang Park,³ Si-in Kim,¹ Hong-Seok Kim,⁴ Yong-Joo Doh,^{4,} Jinhee Kim,^{5,*} Bongsoo Kim^{1,*}*

¹Department of Chemistry, KAIST, Daejeon 34141, Korea

²Department of Physics, Pohang University of Science and Technology, Pohang 37673,
Korea

³Department of Measurement and Analysis, National Nanofab Center, Daejeon 34141,
Korea

⁴Department of Applied Physics, Korea University Sejong Campus, Sejong 30019, Korea

⁵Korea Research Institute of Standards and Science, Daejeon 34113, Korea

[†]These authors contributed equally to this work.

*E-mail: (B.K.) bongsoo@kaist.ac.kr; (J.K.) jinhee@kriss.re.kr; (Y.J.D) yjdoh@korea.ac.kr

ABSTRACT

Single-crystalline β -Ag₂Se nanostructures, a new class of 3D topological insulators (TIs), were synthesized using the chemical vapor transport method. The topological surface states were verified by measuring electronic transport properties including the weak antilocalization effect, Aharonov-Bohm oscillations, and Shubnikov-de Haas oscillations. First-principles band calculations revealed that the band inversion in β -Ag₂Se is caused by strong spin-orbit coupling and Ag-Se bonding hybridization. These extensive investigations provide new meaningful information about silver-chalcogenide TIs that have anisotropic Dirac cones, which could be useful for spintronics applications.

KEYWORDS: anisotropic topological insulator, β -Ag₂Se nanowire, weak antilocalization, Aharonov-Bohm oscillation, Shubnikov-de Haas oscillation, band inversion

Topological insulators (TIs) are bulk insulators with metallic surface states that are topologically protected by time-reversal symmetry.¹ The strong spin-orbit coupling (SOC) inherent to TIs causes the spin orientation of the surface electrons to be locked perpendicular to their translational momentum, resulting in the suppression of electron backscattering from nonmagnetic perturbations.² The formation of spin-textured metallic edge states in TIs enables highly coherent charge and spin transport, making TIs promising for spintronics applications.³ Combinations of TIs with conventional superconductors can also provide useful platforms for creating and manipulating emergent particles such as Majorana fermions,^{4,5} which are essential for topological quantum computers.⁶

The topological surface states (TSSs) in three-dimensional (3D) TIs form two-dimensional (2D) electron gases populated by massless Dirac fermions with spin-momentum locking.⁷ Photoemission spectroscopy⁸⁻¹¹ and electrical transport measurements¹²⁻²⁰ have been used to investigate the TSSs in 3D TIs such as $\text{Bi}_x\text{Sb}_{1-x}$, Bi_2Se_3 , and Bi_2Te_3 , which have isotropic Dirac cones. TSSs with highly anisotropic Dirac cones,²¹ which would be useful for realizing ideal quantum wires exhibiting one-directional spin and electron transport on their surfaces,²² are theoretically expected in silver chalcogenides (Ag_2Se and Ag_2Te).²³ Experimental works, however, have been reported only quite recently on the electronic transport of anisotropic Dirac fermions in silver chalcogenides TIs.^{24,25}

Herein, we report the observation of TI properties in nanowires (NWs) and nanoribbons (NRs) of $\beta\text{-Ag}_2\text{Se}$. We synthesized single-crystalline NWs, NRs, and nanoplates (NPLs) of $\beta\text{-Ag}_2\text{Se}$ using the chemical vapor transport (CVT) method and measured quantum electrical transport properties of $\beta\text{-Ag}_2\text{Se}$ NWs and NRs at low temperatures. Negative magnetoconductance (MC) was observed, indicating the presence of the weak antilocalization (WAL) effect and implying the existence of strong SOC. When a magnetic

field was applied parallel to the NW axis, the β -Ag₂Se NW device exhibited highly periodic MC oscillations, implying the existence of the surface electronic states. When a magnetic field was applied perpendicular to the NW axis, quantum magnetic oscillations, the so-called Shubnikov-de Haas (SdH) oscillations, were observed. The analysis of the SdH oscillations indicates the presence of a nonzero Berry phase due to the TSS of the β -Ag₂Se nanostructure. First-principles band structure calculations confirmed the existence of the TSS.

Because of their anisotropic space and violation of rotational invariance, anisotropic TIs can be potentially employed for observation of exotic fermion through its spaces.^{21,26} Since the in-depth studies for anisotropic TI are quite rare, detailed investigations of these TIs could provide valuable insight into their exotic electrical transport properties, and may allow their possible applications for spintronics and quantum information applications.

RESULTS AND DISCUSSION

Single crystalline β -Ag₂Se nanostructures were synthesized on a *c*-Al₂O₃ substrate using the single-step CVT method (Figure S1, Supporting Information), which enables high quality stoichiometry and assures clean surfaces of the nanostructures.²⁷ The cross-section of the NW had a hexagonal shape, with a diameter of 100 – 250 nm (Figure 1). NRs and NPLs were also synthesized on the same substrates. The widths of the NRs were about 0.4 – 3 μ m and their lengths were 3 – 40 μ m, while NPLs had edge lengths of 3 – 10 μ m.

We performed detailed structural and compositional analyses of the β -Ag₂Se NWs using cross-sectional transmission electron microscopy (TEM). The high-resolution TEM (HRTEM) image and selected-area electron diffraction (SAED) pattern reveal the $[10\bar{1}]$ growth direction and the single crystalline nature of the NW (Figure 1e, f). Lattice spacings of 0.719 nm and 0.383 nm agree well to those of the (010) and (101) planes of an orthorhombic β -

Ag₂Se crystal structure, respectively. All peaks in the X-ray diffraction (XRD) pattern of the synthesized sample are indexed to the orthorhombic β -Ag₂Se phase (space group P2₁2₁2₁, JCPDS card No. 01-071-2410) with a set of lattice constants of $a = 4.333 \text{ \AA}$, $b = 7.062 \text{ \AA}$, $c = 7.764 \text{ \AA}$ (Figure S2, Supporting Information). Additional TEM analyses and TEM energy dispersive X-ray spectroscopy (EDS) measurements also confirmed that all of the synthesized nanostructures are single-crystalline with a Ag/Se atomic ratio of 2:1 (Figure S3, Supporting Information). Details of the NW growth, device fabrications, and the electrical measurements are described in Methods.

We measured five representative β -Ag₂Se NW and NR samples to observe quantum electronic transports. Physical parameters of the samples (**D1** ~ **D5**) are listed in Table S1 (Supporting Information). Figure 2a shows a SEM image of Sample **D1**. Angle-dependent MC curves are obtained at $T = 2.0 \text{ K}$ (Figure 2b). Magnetic field was applied at four different angles (θ). The observed MC is negative, a typical feature of WAL,²⁸ and it becomes more negative as the perpendicular component of the magnetic field increases (with increasing θ). This enhancement of negative MC indicates that the TSS is effective here instead of bulk.^{16,29} Since significant negative MC already exists when $\theta = 0^\circ$, which is attributable to the strong SOC in the bulk portion, we extracted the surface state contribution by subtracting the axial MC component from the total MC, $\Delta G(\theta, B) = G(\theta, B) - G(\theta = 0^\circ, B)$. When the ΔG curves were replotted as functions of the perpendicular magnetic field $B \sin \theta$, they mapped onto a single curve at low magnetic fields (Figure 2c). This extracted term is attributed to the surface states contribution.^{16,17,29}

The low-field $\Delta G(\theta = 90^\circ, B)$ curve was fitted to the 2D WAL model,²⁸ resulting in a phase coherence length L_ϕ of 270 nm at $T = 2.0 \text{ K}$ (Figure S4, Supporting Information). This estimated value of L_ϕ , however, is much larger than the width (w) of the NW, 102 nm,

invalidating the 2D theoretical assumption of $w \gg L_\phi$. We therefore used a diffusive 1D localization model for further analysis,^{17,30,31} including the electron-electron and spin-orbit scatterings:

$$\Delta G = \frac{\sqrt{2}e^2}{\pi\hbar} \frac{L_N}{L} \left[\frac{3}{2} \frac{\text{Ai}\left(\frac{2L_N^2}{L_1^2}\right)}{\text{Ai}'\left(\frac{2L_N^2}{L_1^2}\right)} - \frac{1}{2} \frac{\text{Ai}\left(\frac{2L_N^2}{L_2^2}\right)}{\text{Ai}'\left(\frac{2L_N^2}{L_2^2}\right)} \right] \quad (1)$$

where e is the electric charge, \hbar is the reduced Planck's constant, L is the length of the NW channel, L_N is the Nyquist scattering length,³² Ai is the Airy function, and Ai' is its derivative. Here, $L_1 = \left(\frac{1}{L_\phi^2} + \frac{4}{3L_{\text{so}}^2} + \frac{1}{3} \left(\frac{ewB}{\hbar} \right)^2 \right)^{-\frac{1}{2}}$ and $L_2 = \left(\frac{1}{L_\phi^2} + \frac{1}{3} \left(\frac{ewB}{\hbar} \right)^2 \right)^{-\frac{1}{2}}$, where L_{so} is the spin-orbit scattering length.¹⁷ The fitting results are shown in Figure 2d, yielding $L_\phi = 310$ nm, $L_N = 240$ nm, and $L_{\text{so}} = 200$ nm for the ΔG curve obtained at $T = 2.0$ K. L_ϕ and L_N are comparable to those obtained previously from a Bi_2Se_3 NR, while L_{so} here is about five times larger than that of the Bi_2Se_3 NR.¹⁷ A relatively large L_{so} in the TSS of the β - Ag_2Se NW indicates a more reduced SOC strength than in other TI NWs.^{17, 29}

When the temperature increases, the ΔG curve broadens and diminishes due to increased thermal scattering (Figure 2d). The temperature dependences of the scattering lengths were obtained by fitting the $\Delta G(\theta = 90^\circ, B)$ data to Eq. (1), exhibiting power-law behavior (Figure 2e). It is inferred that L_ϕ , L_N , and L_{so} are proportional to $T^{-0.29}$, $T^{-0.31}$, and $T^{-0.27}$, respectively. Compared with the theoretical expectations,³⁰ according to which L_ϕ and L_N would decay with $T^{-1/3}$ in 1D and $T^{-1/2}$ in 2D, the exponents obtained in our experiment are significantly closer to the prediction by 1D localization theory than that by 2D localization theory.

Measurement of the axial MC by applying a magnetic field B_{axial} along the NW axis confirmed the existence of metallic surface states in the β -Ag₂Se NW. After subtracting a smooth background signal from the MC curve (inset of Figure 3b), regular periodic oscillations with a differential conductance δG were obtained (Figure 3a). The peak position of δG matches well to a linear fit with the integer index n (Figure 3b), indicating that the average period of the δG oscillations is $\Delta B_{\text{axial}} = 0.40$ T. FFT analysis of the $\delta G(B_{\text{axial}})$ curve also resulted in the same oscillation period. Assuming that the NW has a rectangular cross section (139 nm width and 75 nm height, Figure 3c), the cross sectional area becomes 1.04×10^{-14} m². Thus, the oscillation period corresponds to a magnetic flux Φ of $1.01\Phi_0$, where $\Phi_0 = h/e$ is the magnetic flux quantum. Similar Φ_0 -periodic oscillations were obtained using Sample **D5** (Figure S5, Supporting Information).

The periodic MC oscillations can be attributed to the phase-coherent propagation of the surface state electrons around the perimeter of the TI NW,^{12,24,33} which is well known as the Aharonov-Bohm (AB) effect.³⁴ However, there is a significant difference^{35,36}: although AB theory predicts MC minima occurring at integer multiples of Φ_0 , TI NW experiments have shown MC maxima. Moreover, the periodicity can decrease to half of Φ_0 , depending on the gate voltage.¹³ A more plausible explanation than the AB effect is based on the formation of 1D subbands in the TI NW surface states and the nontrivial Berry phases of the surface-state electrons.^{13,36} Since the 1D bandgap³⁶ has been estimated to be $\Delta_{1D} = hv_F/2(w + t) \approx 2.9$ meV, where v_F is the Fermi velocity, w is the width and t is the height of NW,²³ the thermal broadening effect was neglected in our experiment (we assumed $\Delta_{1D} \gg k_B T$). In the regime of weak disorder and nonzero doping, theoretical calculations result in MC oscillations with a period of Φ_0 and doping-dependent conductance maxima either at $n\Phi_0$ or at $(n + 1/2)\Phi_0$, where n is an integer.³⁶ Since the circumference of the NW, $2(w + t)$, was much larger than

the mean free path ($l_e \approx 20$ nm) and its conductance exhibited very weak gate dependence, our β -Ag₂Se NW was in the diffusive regime and away from the Dirac point, thus meeting the conditions assumed in the theoretical calculations.³⁵ The absence of $\Phi_0/2$ -periodic oscillations in Figure 3d indicates that the TI NW was weakly disordered.

In addition to the above MC oscillations, magnetic quantum oscillations such as SdH oscillations constitute the most convincing evidence of surface electronic states.³⁷ Figure 4a shows magnetoresistance (MR) data obtained at a perpendicular magnetic field ($\theta = 90^\circ$). After subtracting the smooth background, we obtained the SdH oscillation of the differential resistance ΔR as a function of $1/B$ (Figure 4b). The FFT analysis result (Figure 4b inset) indicates an oscillation frequency B_f of 84.0 T. Since the oscillation period corresponds to $\Delta(1/B) = 1/B_f = 2\pi e/\hbar S_F$, where $S_F = \pi k_F^2$ is the cross-sectional Fermi surface area transverse to the applied field and k_F is the Fermi wave vector, k_F becomes 0.51 nm^{-1} . Thus, the 2D carrier concentration at the surface was $n_s = k_F^2/4\pi = 2.0 \times 10^{12} \text{ cm}^{-2}$ for the sample **D3**.

According to Lifshitz-Kosevich (LK) theory,³⁸ ΔR is given by $\Delta R = A \exp(-\pi/\mu B) \cos[2\pi(B_f/B + 1/2 + \gamma)]$, where A is a temperature-dependent parameter, μ is the carrier mobility, and $2\pi\gamma$ is the Berry phase. The phase shift is expected to be $\gamma = 0$ for a conventional 2D electron gas and $\gamma = -0.5$ for 2D Dirac electrons.³⁹ Our experimental ΔR data are well fitted by the LK theory with $\mu = 560 \text{ cm}^2 \cdot \text{V}^{-1} \cdot \text{s}^{-1}$ and $\gamma = -0.43$ (see the magenta curve in Figure 4b), supporting the existence of a Berry phase of π due to the TSS. We obtain the elastic mean free path as $l_e = \hbar\mu k_F/e = 19 \text{ nm}$ and $k_F l_e = 9.4$. The SdH oscillations is also observed in the sample **D4** having a different geometry (Figure 4c). Sample **D4** also results in similar physical parameters of n_s , μ , and γ (see Table 1).

The phase factor γ was determined by analyzing the Landau levels (LLs), which are formed by the Landau quantization of the energy states in the magnetic fields. When the ΔR minima in the SdH oscillations are taken to be integer indices (N_{LL}) of the LLs,¹⁹ massless Dirac fermions are expected to satisfy $N_{LL} = B_f/B - 0.5$. Landau fan diagrams are shown in Figure 4d for two different samples. Linear fitting of the fan diagrams revealed a slope B_f of 84.7 T and an intercept γ of -0.56 for the sample **D3**. Parameters for sample **D4** are B_f of 122.0 T and γ of -0.42 ; these values are quite close to those estimated from the previous analyses based on the LK theory. Thus, our experimental results suggest that β -Ag₂Se NWs contain massless Dirac fermions with Berry phases of π on their surfaces.

To clarify the nontrivial topological property of β -Ag₂Se, we performed the first-principles calculations based on the density functional theory.^{40,41} The ionic character of Ag-Se bonding implies that the Ag-cation s states lie higher in energy than the Se-anion p states. The strong hybridization between Ag d states and Se p states, however, leads to the band inversion, as in Ag₂Te.²³ The strength of the p - d hybridization depends on the number of bonding neighbors of chalcogen atoms (seven for β -Ag₂Se and eight for α -Ag₂Te). Thus the Ag s states are located at about -1.25 eV below the Fermi level, while the Se p states are above them (Figure 5b). Our band-structure calculation for a 15.53 nm-thick β -Ag₂Se slab (Figure 5c) reveals that the bulk band gap is opened by the SOC and the surface states (red lines) with a linear dispersion develop inside the gap. Without SOC, the gap is closed and the surface states disappear. Figure 5d shows that the surface states are localized at the top and bottom surfaces of the β -Ag₂Se slab. These calculation results are consistent with our experimental measurements, both providing evidences for the existence of TSSs in β -Ag₂Se NWs.

The topological nature of β -Ag₂Se can be confirmed by calculating the Wannier charge centers (WCCs) on the six faces of the first Brillouin zone. Figures 5e and 5f display the

evolution of WCCs for the $k_y = 0$ and $k_y = \pi$ faces, respectively, by varying the pumping parameter k_x . As shown, the evolution curves (red solid curves) cross an arbitrary reference line (black dashed line) odd numbers of times on the k_x , k_y , and $k_z = 0$ faces and even numbers of times on the k_x , k_y , and $k_z = \pi$ faces. The odd numbers of crossings indicate that the Kramer pairs with time-reversal-invariant momenta exchange their partners during the pumping process, demonstrating the nontrivial topological nature of the material.^{42, 43} Our calculation results show that the topological index of β -Ag₂Se is 1;(0,0,0), supporting the suggestion of β -Ag₂Se as a new class of 3D TI.⁴⁴

CONCLUSIONS

We synthesized single-crystalline β -Ag₂Se nanostructures and studied their electrical transport properties. We observed the WAL effect, AB oscillations, and SdH oscillations, all of which support the existence of the conducting surface states and thus the TI nature of this material. Our analysis indicated that the β -Ag₂Se NWs had a nonzero Berry phase as a characteristic property of massless Dirac fermions. First-principles calculations confirmed the existence of TSSs in this material. As a new TI, β -Ag₂Se could provide a useful platform for studying the exotic electronic transport due to the anisotropic Dirac cone and for developing novel spintronic devices.

EXPERIMENTAL METHODS

Synthesis. Single crystalline β -Ag₂Se NWs, NRs and NPLs were synthesized in a horizontal hot-wall two-zone furnace with a 1 inch diameter inner quartz tube, as shown in Figure S1 (Supporting information). Ag₂Se powder of 0.02 g (Sigma-Aldrich) in an alumina boat was placed at the center of the upstream (US) zone. And sapphire (*c*-Al₂O₃) substrates were placed at ~ 30 cm downstream (DS) from the boat. The carrier Ar gas was supplied through a mass-flow controller at a rate of 30 sccm. The temperatures of the US zone and DS zone were maintained at 900 °C and 950 °C, respectively. The reaction time was 40 minutes, while the pressure was maintained at 3.6 Torr during the reaction.

Characterization. SEM images of β -Ag₂Se nanostructures were taken on a Nova 230 (FEI Co.). The XRD pattern of the as-grown nanostructures was recorded on a RIGAKU D/MAX-RC (12 kW) diffractometer operated at 30 kV and 60 mA with filtered CuK_α radiation. TEM, HRTEM images, SAED patterns and EDS spectra were taken by a JEOL JEM-2100F TEM (200 kV operation) and a FEI Tecnai G2 F30 (300 kV).

Device fabrication and transport measurement. A single β -Ag₂Se NW was transferred from a sapphire substrate to a SiO_x coated Si substrate with pre-patterned Ti/Au pad. Conventional electron-beam lithography and RF sputtering were used to form Ti (15 nm)/Au (150 nm) electrodes. The e-beam resist, poly (methyl methacrylate) (PMMA 4% 950 K) was baked at 170 °C for 2 min. The MR was measured using a Physical Properties Measurement System (PPMS, Quantum Design Inc.) equipped with a rotating probe. We used a conventional four-probe measurement configuration combined with AC lock-in technique.

Computational methods. All calculations were performed using the first-principles methods based on the density functional theory as implemented in the Vienna *ab initio* simulation package (VASP)⁴⁵⁻⁴⁷ (for β -Ag₂Se bulk) and the OpenMX codes⁴⁸⁻⁵⁰ (for β -Ag₂Se

slab). The exchange-correlation energy functional was treated with the generalized gradient approximation parameterized by Perdew, Burke and Enzelhof.⁵¹ For bulk calculations, we used the projector augmented wave pseudopotentials⁵² provided by VASP. We selected 400 eV as the energy cutoff for the plane-wave basis set. For slab calculations, we used the norm conserving pseudopotentials proposed by Morrison, Bylander, and Kleinman.⁵³ The pseudo-atomic basis orbitals are chosen as Ag7.0-s2p2d1 and Se7.0-s2p2d1. The lattice parameters of β -Ag₂Se were determined experimentally ($a = 4.333 \text{ \AA}$, $b = 7.062 \text{ \AA}$, and $c = 7.764 \text{ \AA}$)⁵⁴ and the first Brillouin zone was integrated using Γ -centered $16 \times 10 \times 9$ k-point samplings for bulk and $9 \times 6 \times 1$ for slab.

ACKNOWLEDGMENTS

B.K. acknowledges support of this work from National Research Foundation grant (NRF-2013R1A2A2A01069073). Y.J.D acknowledges support of this work from National Research Foundation of Korea through the Basic Science Research Program (Grant No. 2015R1A2A2A01006833). We are grateful to Kicheon Kang for useful discussions.

Supporting information available

FIGURE CAPTIONS

Table 1. Physical parameters of the surface states obtained from the LK analysis of SdH oscillations.

Sample	B_f (T)	μ ($\text{cm}^2\text{V}^{-1}\text{s}^{-1}$)	γ	n_s (cm^{-2})	k_F (nm^{-1})	l_e (nm)
D3	84.0	560	-0.43	2.0×10^{12}	0.51	19
D4	122	580	-0.55	3.0×10^{12}	0.61	23

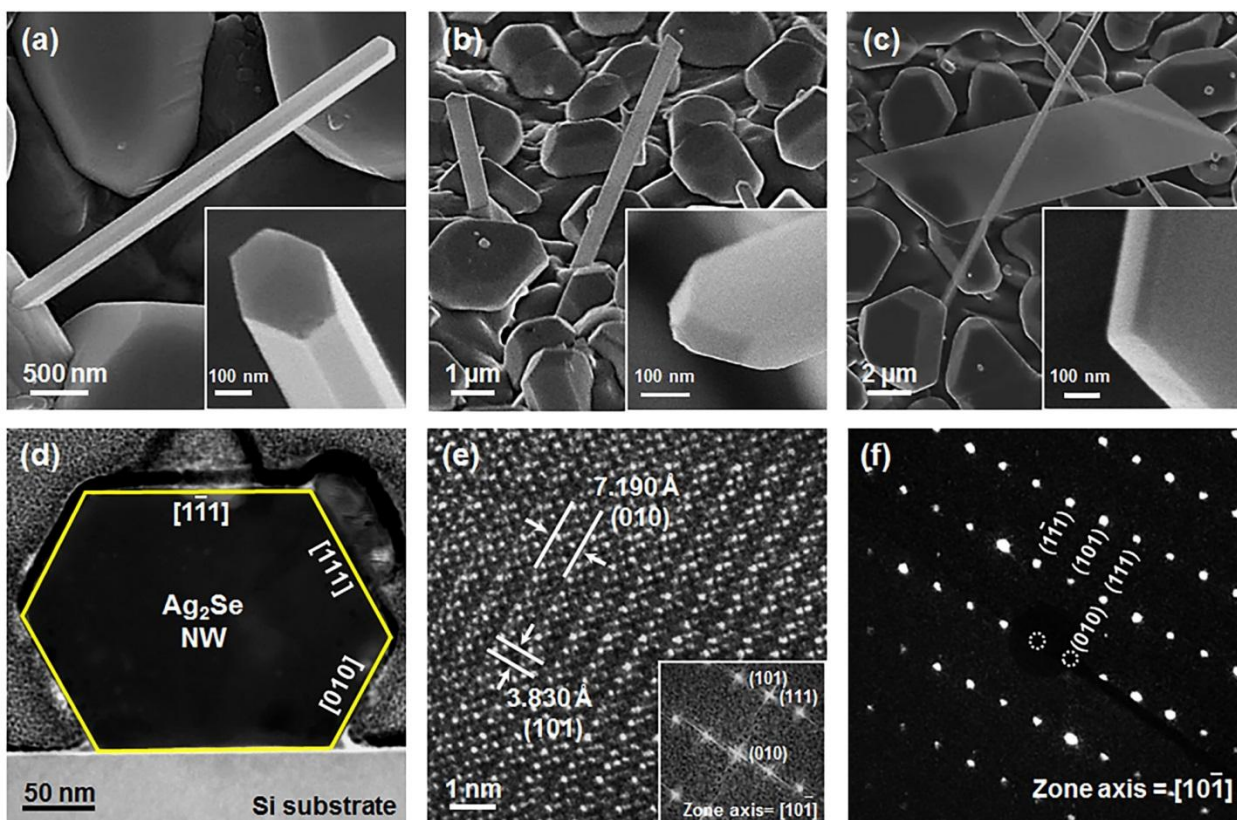


Figure 1. SEM images of as-synthesized β - Ag_2Se (a) NW, (b) NR and (c) NPL on a $c\text{-Al}_2\text{O}_3$ substrate. The insets in (a), (b) and (c) are magnified SEM images of the each nanostructures. (d) Cross-sectional TEM image of a β - Ag_2Se NW. (e) HRTEM image of (d). The FFT pattern (inset in (e)) is indexed to β - Ag_2Se with an orthorhombic lattice along the $[10\bar{1}]$ zone axis. (f) SAED pattern of a β - Ag_2Se NW along the $[10\bar{1}]$ zone axis.

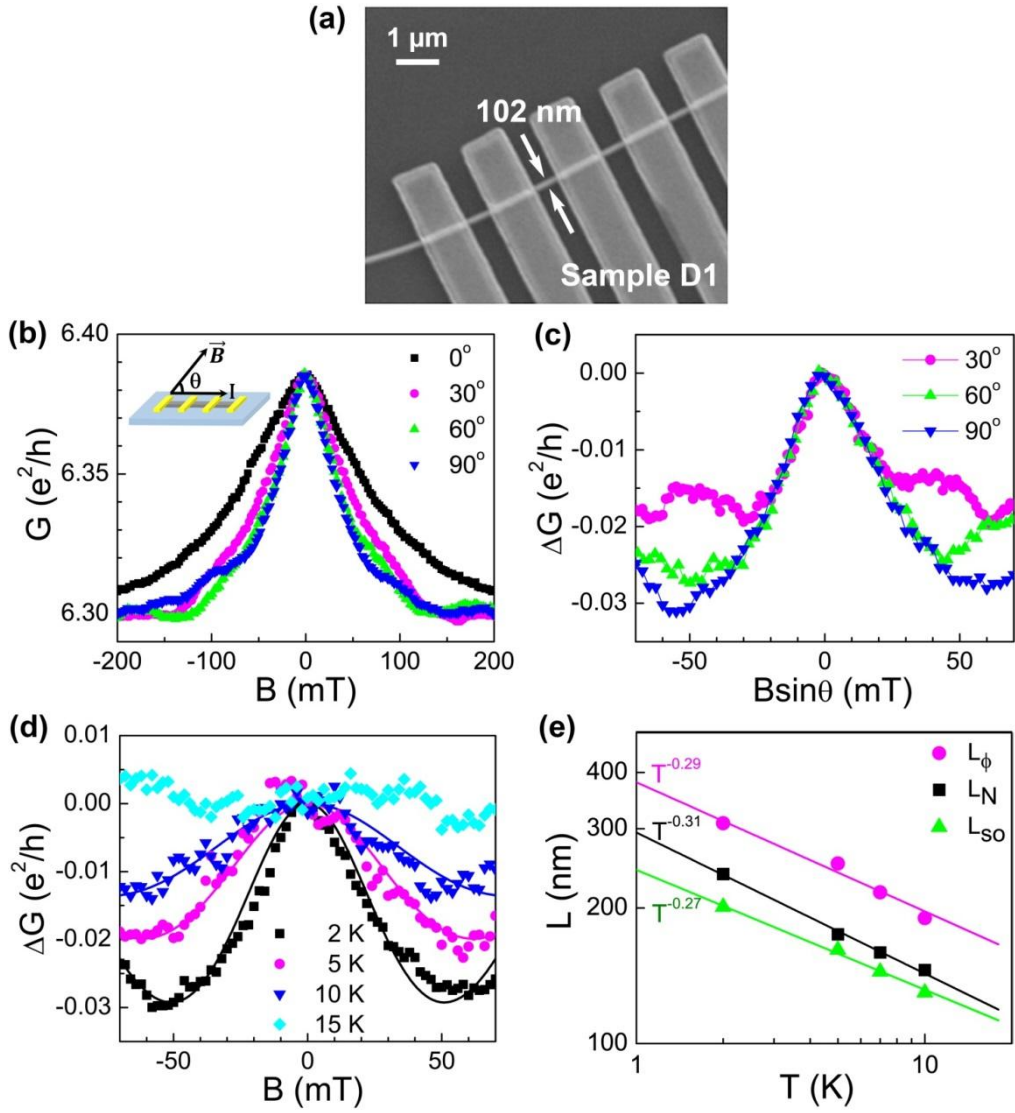


Figure 2. (a) SEM image of the β -Ag₂Se NW device (Sample **D1**) with a NW width of 102 nm (b) Angle-dependent MC curves at $T = 2.0$ K. Magnetic field was applied at various angles θ relative to the NW axis. Inset: Schematic of the measurement configuration. (c) Angle-dependent differential MC $\Delta G = G(\theta) - G(\theta=0^\circ)$, versus perpendicular component of magnetic field, $B\sin\theta$. (d) Temperature dependence of $\Delta G(B)$ curve (symbols). Solid curves are fitting results obtained by using 1D WAL theory. (e) Characteristic lengths of L_ϕ , L_N , and L_{so} as functions of temperature. Solid lines are results of power-law fits.

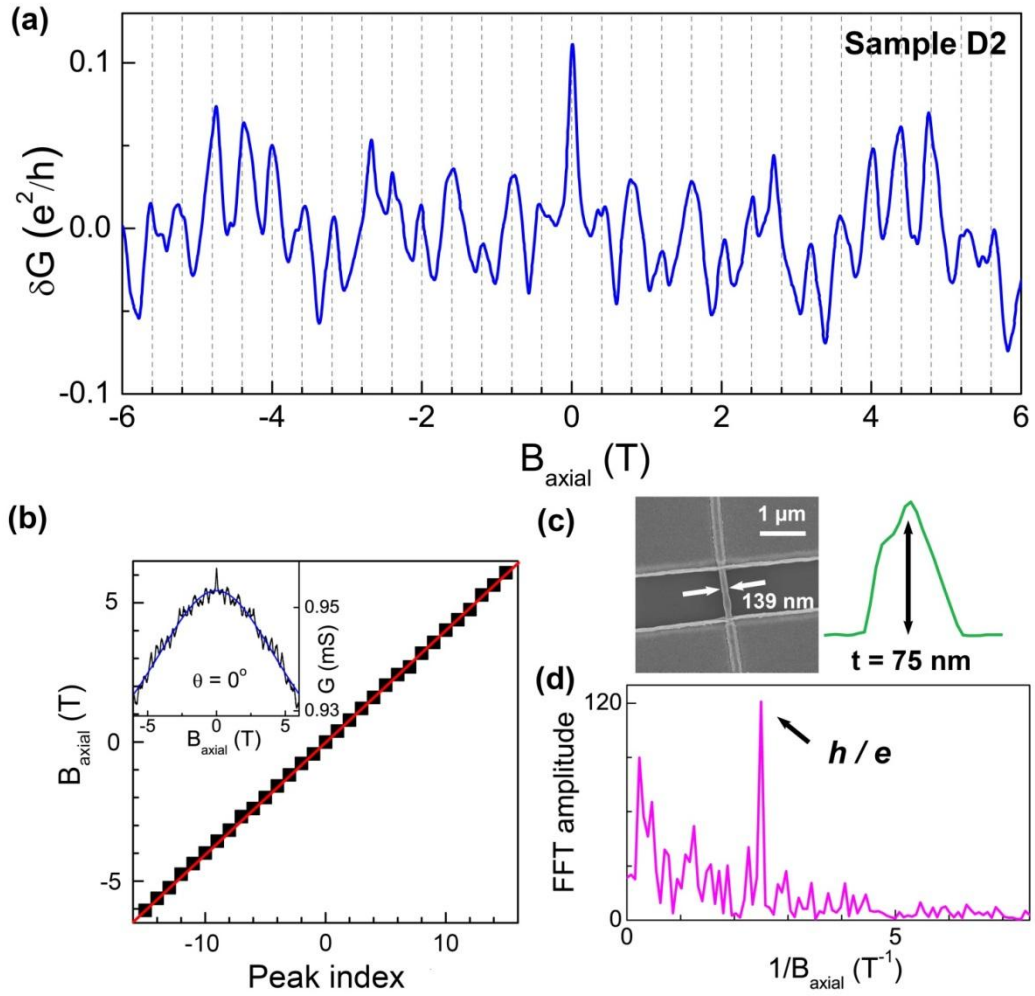


Figure 3. (a) Differential MC at $T = 2.0$ K after subtracting smooth background. The dotted lines indicate an average period $\Delta B_{\text{axial}} = 0.40$ T for the oscillation. (b) Magnetic field positions of δG maxima versus integer index. Solid line is a linear fit. Inset: Raw data of axial MR obtained from sample **D2**. Blue curve is smoothly varying background. (c) Left : SEM image of a NW device with a NW width of 139 nm. Right: The height of the NW is 75 nm as determined by AFM. (d) FFT of $\delta G(B_{\text{axial}})$ curve in (a). Peak location, $1/B_{\text{axial}} = 2.499$ T⁻¹, corresponds to h/e oscillations.

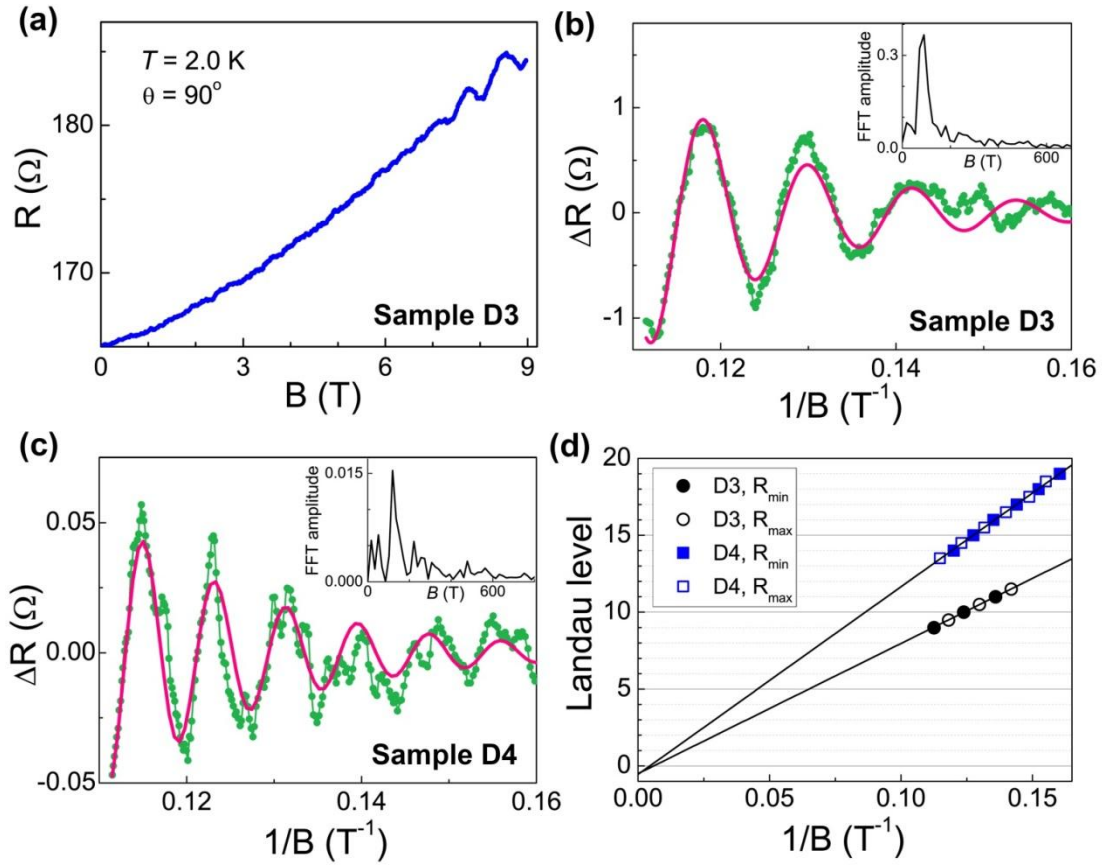


Figure 4. (a) MR data obtained from sample **D3** with a magnetic field perpendicular to the substrate. (b) Differential MR after subtracting smooth background. Solid magenta curve is a fit to LK theory (see text). Inset: FFT of ΔR with peak at $B_f = 84.0$ T. (c) ΔR obtained from sample **D4**. Solid magenta curve shows fitting result. Inset: FFT of ΔR with peak at $B_f = 122$ T. (d) Landau level index versus $1/B$ value obtained from sample **D3** (black) and **D4** (blue). ΔR minima (maxima) correspond to integer (half-integer) values of Landau level index. Lines are linear least square fits to data.

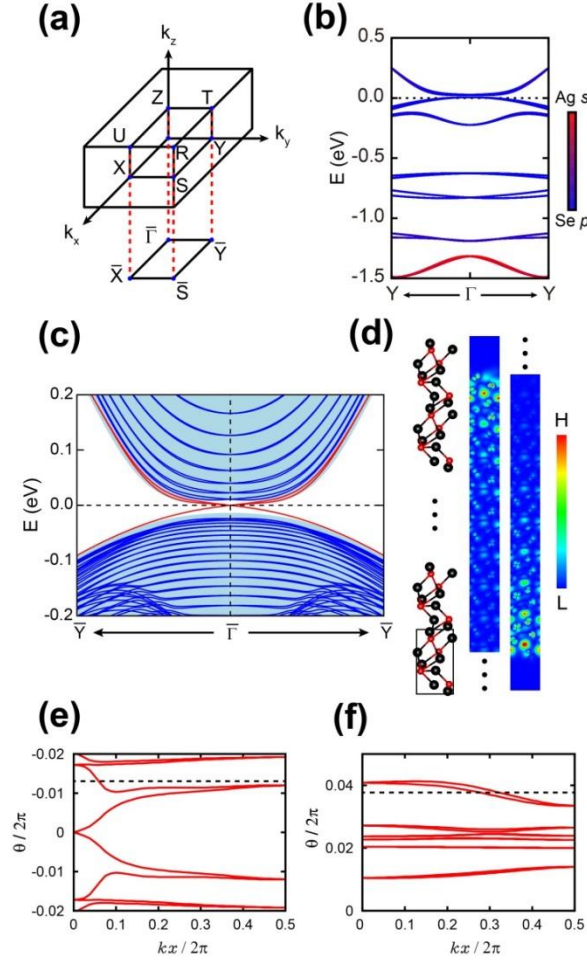


Figure 5. (a) First Brillouin zone of orthorhombic β - Ag_2Se and its 2D-projected surface Brillouin zone. (b) Contribution of Ag s (red) and Se p (blue) states to band structure of β - Ag_2Se . Bands from Ag s states (located about -1.25 eV) exhibit band-inversion feature. (c) Surface states in 15.53 nm-thick, c -axis normal β - Ag_2Se slab (red curve) with the (projected) bulk bands in blue curves (shaded light blue). (d) Part of β - Ag_2Se slab (left panel: Ag, black; Se, red) and surface-localized states of top (center panel) and bottom (right panel) surfaces at Γ . Evolution of Wannier charge centers in (e) $k_y = 0$ and (f) $k_y = \pi$ faces.

REFERENCES AND NOTES

1. Hasan, M. Z.; Kane, C. L. Colloquium: Topological insulators. *Rev. Mod. Phys.* **2010**, *82*, 3045–3067.
2. Moore, J. E. The birth of topological insulators. *Nature* **2010**, *464*, 194–198.
3. Li, C. H.; van 't Erve, O. M.; Robinson, J. T.; Liu, Y.; Li, L.; Jonker, B. T. Electrical detection of charge-current-induced spin polarization due to spin-momentum locking in Bi_2Se_3 . *Nat. Nanotechnol.* **2014**, *9*, 218–24.
4. Qi, X.-L.; Zhang, S.-C. Topological insulators and superconductors. *Rev. Mod. Phys.* **2011**, *83*, 1057.
5. Beenakker, C. W. J. Search for Majorana fermions in superconductors. *Annu. Rev. Con. Mat. Phys.* **2013**, *4*, 113.
6. Alicea, J.; Oreg, Y.; Refael, G.; von Oppen, F.; Fisher, M. P. A. Non-Abelian statistics and topological quantum information processing in 1D wire networks. *Nat. Phys.* **2011**, *7*, 412.
7. Fu, L.; Kane, C.; Mele, E. Topological Insulators in Three Dimensions. *Phys. Rev. Lett.* **2007**, *98*.
8. Hsieh, D.; Qian, D.; Wray, L.; Xia, Y.; Hor, Y. S.; Cava, R. J.; Hasan, M. Z. A topological Dirac insulator in a quantum spin Hall phase. *Nature* **2008**, *452*, 970.
9. Xia, Y.; Qian, D.; Hsieh, D.; Wray, L.; Pal, A.; Lin, H.; Bansil, A.; Grauer, D.; Hor, Y. S.; Cava, R. J.; Hasan, M. Z. Observation of a large-gap topological-insulator class with a single Dirac cone on the surface. *Nat. Phys.* **2009**, *5*, 398–402.
10. Chen, Y. L.; Analytis, J. G.; Chu, J. H.; Liu, Z. K.; Mo, S. K.; Qi, X. L.; Zhang, H. J.; Lu, D. H.; Dai, X.; Fang, Z.; Zhang, S. C.; Fisher, I. R.; Hussain, Z.; Shen, Z. X. Experimental realization of a three-dimensional topological insulator, Bi_2Te_3 . *Science* **2009**, *325*, 178–81.
11. Hsieh, D.; Xia, Y.; Qian, D.; Wray, L.; Dil, J. H.; Meier, F.; Osterwalder, J.; Patthey, L.; Checkelsky, J. G.; Ong, N. P.; Fedorov, A. V.; Lin, H.; Bansil, A.; Grauer, D.; Hor, Y. S.; Cava, R. J.; Hasan, M. Z. A tunable topological insulator in the spin helical Dirac transport regime. *Nature* **2009**, *460*, 1101–5.
12. Peng, H.; Lai, K.; Kong, D.; Meister, S.; Chen, Y.; Qi, X. L.; Zhang, S. C.; Shen, Z. X.; Cui, Y. Aharonov-Bohm interference in topological insulator nanoribbons. *Nat. Mater.*

2010, 9, 225–9.

13. Hong, S. S.; Zhang, Y.; Cha, J. J.; Qi, X.-L.; Cui, Y. One-Dimensional Helical Transport in Topological Insulator Nanowire Interferometers. *Nano Lett.* **2014**, *14*, 2815.
14. Qu, D. X.; Hor, Y. S.; Xiong, J.; Cava, R. J.; Ong, N. P. Quantum oscillations and hall anomaly of surface states in the topological insulator Bi_2Te_3 . *Science* **2010**, *329*, 821–4.
15. Tang, H.; Liang, D.; Qiu, R. L. J.; Gao, X. P. A. Two-Dimensional Transport-Induced Linear Magneto-Resistance in Topological Insulator Bi_2Se_3 Nanoribbons. *ACS Nano* **2011**, *5*, 7510.
16. Cha, J. J.; Kong, D.; Hong, S. S.; Analytis, J. G.; Lai, K.; Cui, Y. Weak antilocalization in $\text{Bi}_2(\text{Se}_x\text{Te}_{1-x})_3$ nanoribbons and nanoplates. *Nano Lett.* **2012**, *12*, 1107–11.
17. Cha, J. J.; Claassen, M.; Kong, D.; Hong, S. S.; Koski, K. J.; Qi, X.-L.; Cui, Y. Effects of Magnetic Doping on Weak Antilocalization in Narrow Bi_2Se_3 Nanoribbons. *Nano Lett.* **2012**, *12*, 4355.
18. Analytis, J. G.; McDonald, R. D.; Riggs, S. C.; Chu, J.-H.; Boebinger, G. S.; Fisher, I. R. Two-dimensional surface state in the quantum limit of a topological insulator. *Nat. Phys.* **2010**, *6*, 960.
19. Sacepe, B.; Oostinga, J. B.; Li, J.; Ubaldini, A.; Couto, N. J.; Giannini, E.; Morpurgo, A. F. Gate-tuned normal and superconducting transport at the surface of a topological insulator. *Nat. Commun.* **2011**, *2*, 575.
20. Kim, H.-S.; Shin, H. S.; Lee, J. S.; Ahn, C. W.; Song, J. Y.; Doh, Y.-J. Quantum electrical transport properties of topological insulator Bi_2Te_3 nanowires. *Curr. Appl. Phys.* **2016**, *16*, 51.
21. Tang, S.; Dresselhaus, M. S. Constructing anisotropic single-Dirac-cones in $\text{Bi}_{(1-x)}\text{Sb}_{(x)}$ thin films. *Nano Lett.* **2012**, *12*, 2021–6.
22. Virost, F.; Hayn, R.; Richter, M.; van den Brink, J. Metacinnabar (β -HgS): A Strong 3D Topological Insulator with Highly Anisotropic Surface States. *Phys. Rev. Lett.* **2011**, *106*.
23. Zhang, W.; Yu, R.; Feng, W.; Yao, Y.; Weng, H.; Dai, X.; Fang, Z. Topological Aspect and Quantum Magnetoresistance of β - Ag_2Te . *Phys. Rev. Lett.* **2011**, *106*.
24. Lee, S.; In, J.; Yoo, Y.; Jo, Y.; Park, Y. C.; Kim, H. J.; Koo, H. C.; Kim, J.; Kim, B.; Wang, K. L. Single crystalline β - Ag_2Te nanowire as a new topological insulator. *Nano Lett.* **2012**, *12*, 4194–9.
25. Sulaev, A.; Zhu, W.; Teo, K. L.; Wang, L. Gate-tuned quantum oscillations of

topological surface states in β -Ag₂Te. *Sci. Rep.* **2015**, *5*, 8062.

26. Park, C. H.; Yang, L.; Son, Y. W.; Cohen, M. L.; Louie, S. G. Anisotropic behaviours of massless Dirac fermions in graphene under periodic potentials. *Nat. Phys.* **2008**, *4*(3), 213–217.
27. Kong, D.; Randel, J. C.; Peng, H.; Cha, J. J.; Meister, S.; Lai, K.; Chen, Y.; Shen, Z.-X.; Manoharan, H. C.; Cui, Y. Topological insulator nanowires and nanoribbons. *Nano Lett.* **2010**, *10*, 329–333.
28. Hikami, S.; Larkin, A. I.; Nagaoka, Y. Spin-Orbit Interaction and Magnetoresistance in the 2 Dimensional Random System. *Prog. Theor. Phys.* **1980**, *63*, 707–710.
29. Ning, W.; Du, H.; Kong, F.; Yang, J.; Han, Y.; Tian, M.; Zhang, Y. One-dimensional weak antilocalization in single-crystal Bi₂Te₃ nanowires. *Sci. Rep.* **2013**, *3*, 1564.
30. Altshuler, B. L.; Aronov, A. G.; Khmelnitsky, D. E. Effects of electron-electron collisions with small energy transfers on quantum localisation. *J. Phys. C: Solid State Phys.* **1982**, *15*, 7367.
31. Alegria, L. D.; Schroer, M. D.; Chatterjee, A.; Poirier, G. R.; Pretko, M.; Patel, S. K.; Petta, J. R. Structural and Electrical Characterization of Bi₂Se₃ Nanostructures Grown by Metal–Organic Chemical Vapor Deposition. *Nano Lett.* **2012**, *12*, 4711.
32. Echternach, P. M.; Gershenson, M. E.; Bozler, H. M. Nyquist phase relaxation in one-dimensional metal films. *Phys. Rev. B* **1993**, *48*, 11516.
33. Xiu, F.; He, L.; Wang, Y.; Cheng, L.; Chang, L.-T.; Lang, M.; Huang, G.; Kou, X.; Zhou, Y.; Jiang, X.; Chen, Z.; Zou, J.; Shailos, A.; Wang, K. L. Manipulating surface states in topological insulator nanoribbons. *Nat. Nanotechnol.* **2011**, *6*, 216.
34. Aharonov, Y.; Bohm, D. Significance of Electromagnetic Potentials in the Quantum Theory. *Phys. Rev.* **1959**, *115*, 485–491.
35. Zhang, Y.; Vishwanath, A. Anomalous Aharonov-Bohm Conductance Oscillations from Topological Insulator Surface States. *Phys. Rev. Lett.* **2010**, *105*, 206601.
36. Bardarson, J. H.; Brouwer, P. W.; Moore, J. E. Aharonov-Bohm Oscillations in Disordered Topological Insulator Nanowires. *Phys. Rev. Lett.* **2010**, *105*, 156803.
37. Taskin, A. A.; Ando, Y. Quantum oscillations in a topological insulator Bi_{1-x}Sb_x. *Phys. Rev. B* **2009**, *80*, 085303.
38. Isihara, A.; Smrcka, L. Density and magnetic field dependences of the conductivity of two-dimensional electron systems. *J. Phys. C: Solid State Phys.* **1986**, *19*, 6777.

39. Bardarson, J. H.; Moore, J. E. Quantum interference and Aharonov-Bohm oscillations in topological insulator. *Rep. Prog. Phys.* **2013**, *76*, 056501.
40. Hohenberg, P. Inhomogeneous Electron Gas. *Phys. Rev.* **1964**, *136*, B864–B871.
41. Kohn, W.; Sham, L. J. Self-Consistent Equations Including Exchange and Correlation Effects. *Phys. Rev.* **1965**, *140*, A1133–A1138.
42. Soluyanov, A. A.; Vanderbilt, D. Computing topological invariants without inversion symmetry. *Phys. Rev. B* **2011**, *83*.
43. Fu, L.; Kane, C. Time reversal polarization and a Z_2 adiabatic spin pump. *Phys. Rev. B* **2006**, *74*.
44. Zhao, Z.; Wang, S.; Oganov, A. R.; Chen, P.; Liu, Z.; Mao, W. L. Tuning the crystal structure and electronic states of Ag_2Se : Structural transitions and metallization under pressure. *Phys. Rev. B* **2014**, *89*.
45. Kresse, G.; Furthmüller, J. Efficiency of ab-initio total energy calculations for metals and semiconductors using a plane-wave basis set. *Comput. Mater. Sci.* **1996**, *6*, 15–50.
46. Kresse, G.; Furthmüller, J. Efficient iterative schemes for ab initio total-energy calculations using a plane-wave basis set. *Phys. Rev. B* **1996**, *54*, 11169–11186.
47. Kresse, G.; Hafner, J. Ab initio molecular dynamics for liquid metals. *Phys. Rev. B* **1993**, *47*, 558–561.
48. Ozaki, T. Variationally optimized atomic orbitals for large-scale electronic structures. *Phys. Rev. B* **2003**, *67*, 155108.
49. Ozaki, T.; Kino, H. Numerical atomic basis orbitals from H to Kr. *Phys. Rev. B* **2004**, *69*, 195113.
50. Ozaki, T.; Kino, H. Efficient projector expansion for the ab initio LCAO method. *Phys. Rev. B* **2005**, *72*, 045121.
51. Perdew, J. P.; Burke, K.; Ernzerhof, M. Generalized Gradient Approximation Made Simple. *Phys. Rev. Lett.* **1996**, *77*, 3865–3868.
52. Kresse, G.; Joubert, D. From ultrasoft pseudopotentials to the projector augmented-wave method. *Phys. Rev. B* **1999**, *59*, 1758–1775.
53. Morrison, I.; Bylander, D. M.; Kleinman, L. Nonlocal Hermitian norm-conserving Vanderbilt pseudopotential. *Phys. Rev. B* **1993**, *47*, 6728–6731.
54. Shimojo, F.; Okazaki, H. Phase Transition in Superionic Conductor Ag_2Se : A Molecular Dynamics Study. *J. Phys. Soc. Jpn.* **1991**, *60*, 3745–3753.

Supporting Information

1. Parameters of nanowires and nanoribbon
2. Experimental setup
3. XRD spectrum
4. TEM analyses of β -Ag₂Se nanowires and nanoplate
5. 2D weak antilocalization fitting result
6. Aharonov-Bohm oscillation

*Address correspondence to bongsoo@kaist.ac.kr, jinhee@kriss.re.kr,
yjdoh@korea.ac.kr

Fax: +82-42-350-2810

Table S1. Parameters of β -Ag₂Se nanowires and nanoribbon samples.

No.	Resistivity at 2 K (m Ω -cm)	Width (nm)	Height (nm)	Channel length (μ m)
D1	5.2	102	95	0.75
D2	1.3	139	75	0.79
D3	0.15	227	150	3.69
D4	0.18	2770	200	11.8
D5	0.40	140	150	0.55

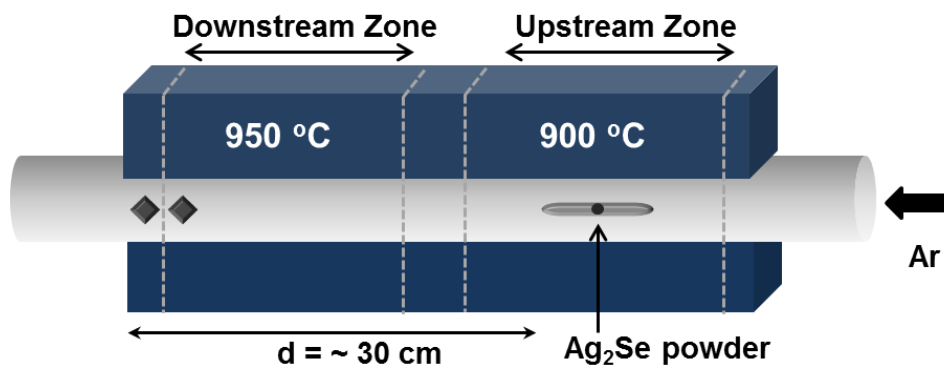


Figure S1. Experimental setup for the synthesis of β - Ag_2Se nanowires (NWs), nanoribbons (NRs) and nanoplates (NPLs).

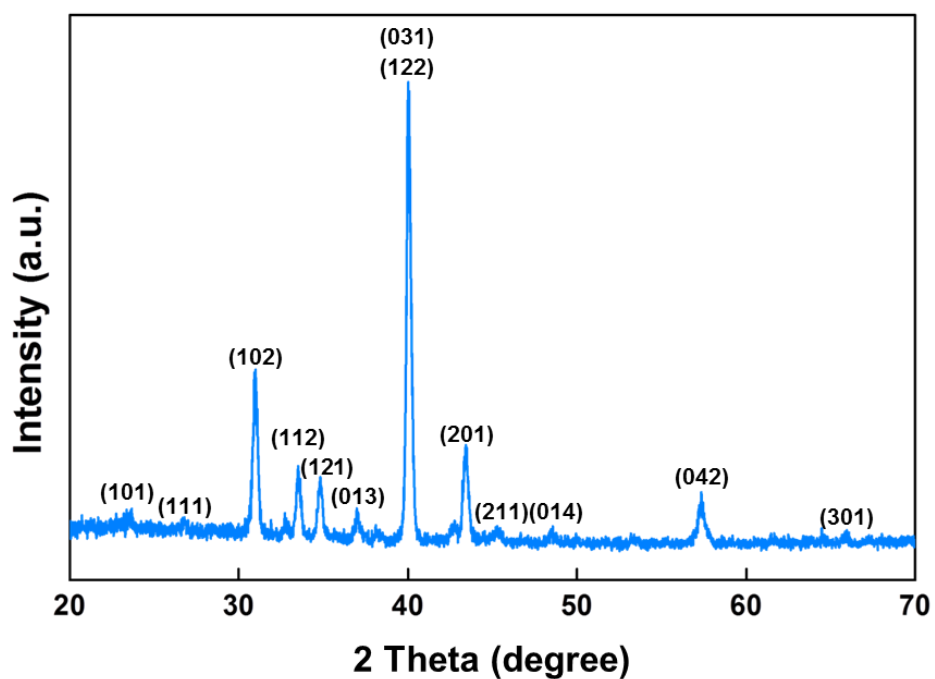


Figure S2. The X-ray diffraction (XRD) pattern obtained from as-grown NWs, NRs and NPLs on $c\text{-Al}_2\text{O}_3$ substrate. All the diffraction peaks are indexed to an orthorhombic $\beta\text{-Ag}_2\text{Se}$ crystal structure (JCPDS card No. 01-071-2410).

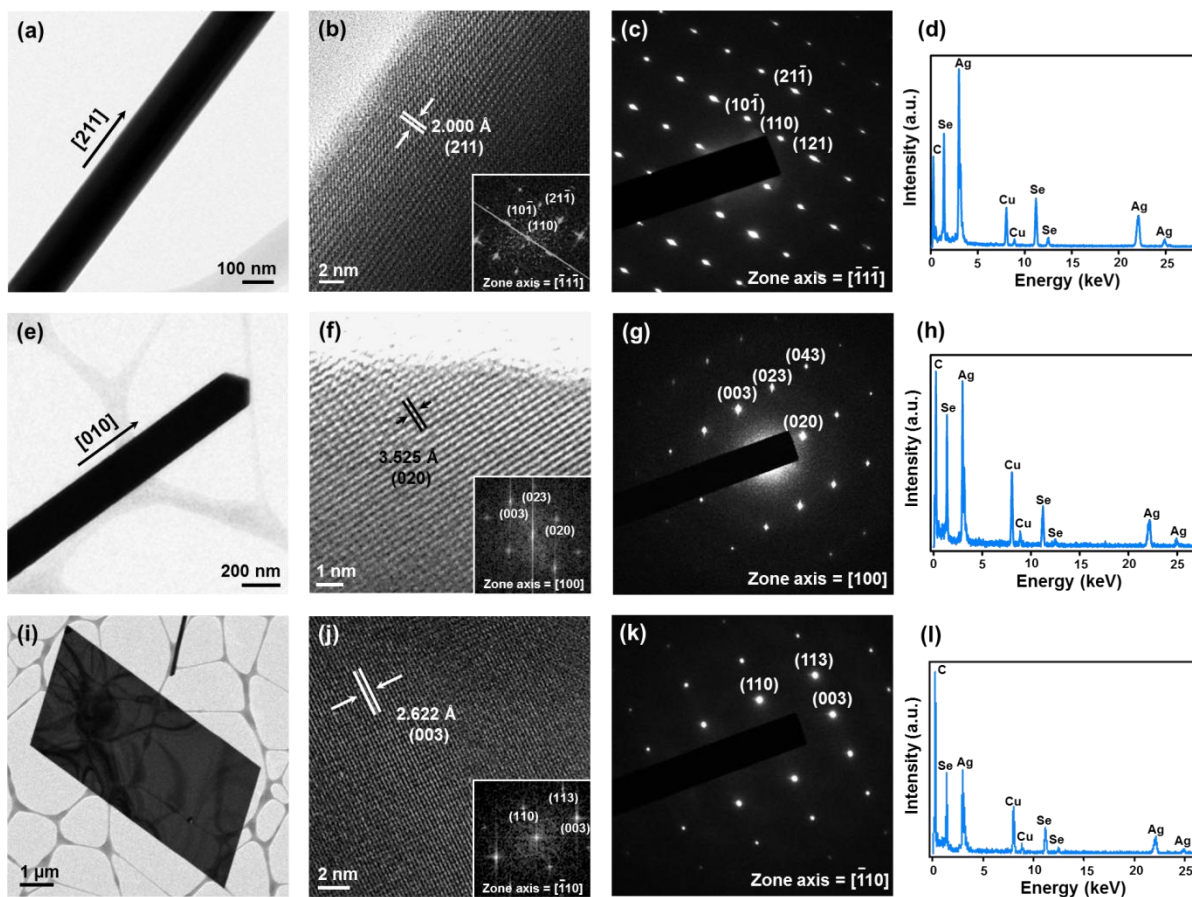


Figure S3. TEM images of β -Ag₂Se NWs and NPL.

First column ((a), (e), (i)): Low-resolution TEM images of the β -Ag₂Se NWs and NPL. Second column ((b), (f), (j)): High-resolution TEM images and FFT patterns (inset image) of β -Ag₂Se NWs and NPL. Lattice spacings of 0.200 nm, 0.353 nm, and 0.262 nm agree well to those of (211), (020), and (003) planes of an orthorhombic β -Ag₂Se crystal structure, respectively. Third column ((c), (g), (k)): The SAED patterns along the various zone axes. The patterns show the single crystalline nature of β -Ag₂Se nanostructures. Fourth column ((d), (h), (l)): TEM-EDS spectra of β -Ag₂Se NWs and NPL. The analyses of these results confirm that the NWs and NPL contain Ag and Se, in a ratio of 2:1. (Cu and C peaks are due to a

TEM grid)

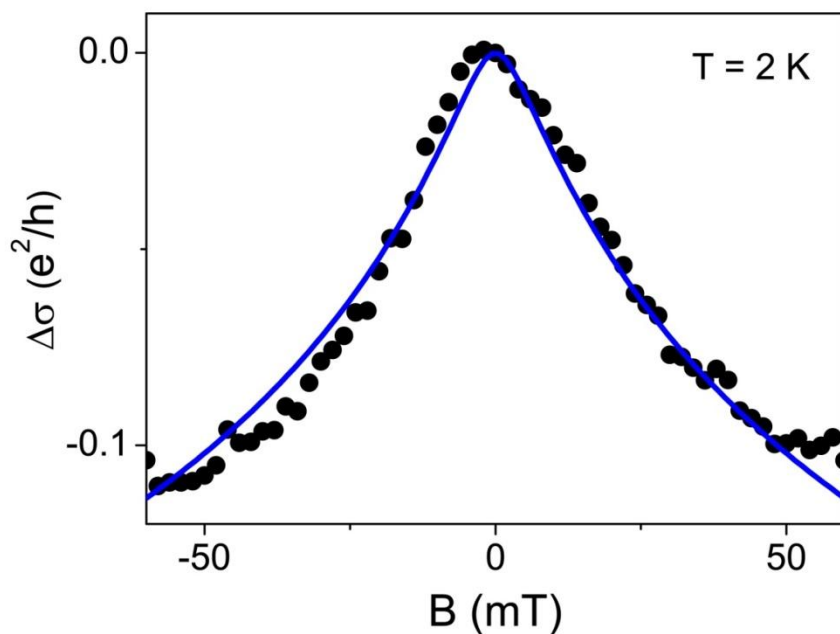


Figure S4. 2D differential magnetoconductance (MC) data (symbol) obtained from sample **D1** at $T = 2.0$ K. Solid line is a fit to the 2D weak antilocalization (WAL) model.¹ The model expects 2D MC $\Delta\sigma = -(\alpha e^2)/(2\pi^2\hbar)[\ln(B_0/B) - \psi(1/2 + B_0/B)]$, where α is a prefactor, $B_0 = \hbar/(4eL_\varphi^2)$, L_φ is a phase coherence length, and ψ is a digamma function. A least square fitting results in $\alpha = 0.25$ and $L_\varphi = 270$ nm.

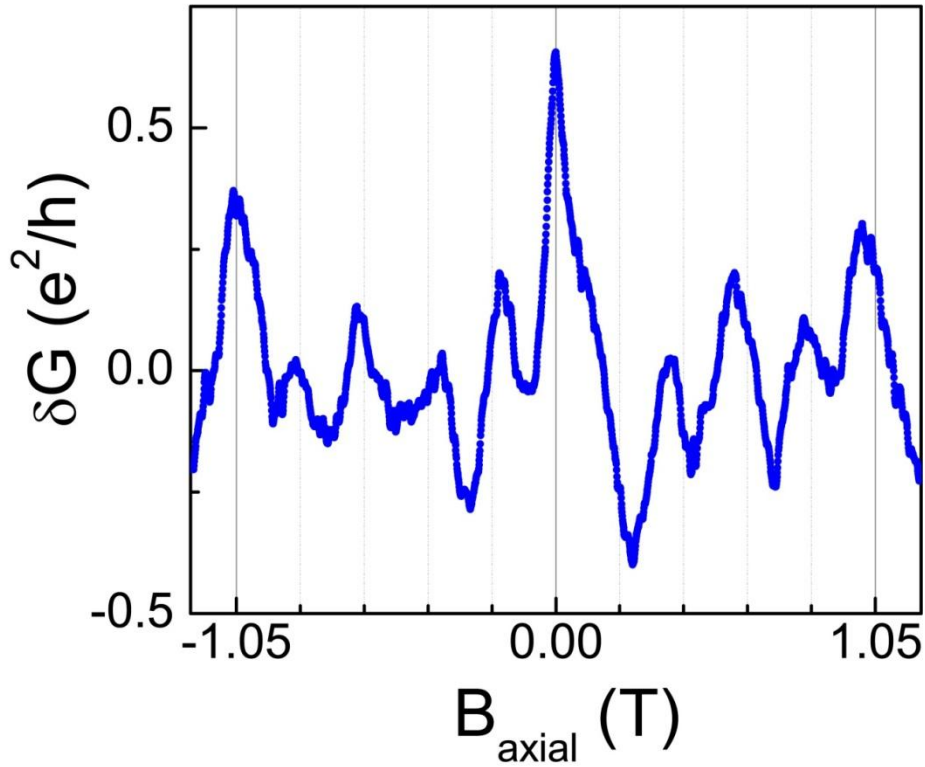


Figure S5. Differential MC obtained from sample **D5** at $T = 2.0$ K. A smooth background MC was subtracted out. The dotted lines indicate an average period $\Delta B_{\text{axial}} = 0.21$ T for the δG oscillations. Assuming that the NW has a rectangular cross section, the area becomes 2.10×10^{-14} m². Thus, the oscillation period corresponds to a magnetic flux $\Phi = 1.07\Phi_0$, where $\Phi_0 = h/e$ is the magnetic flux quantum. The flux can be overestimated by the approximation of the cross sectional shape.

References

1. Hikami, S.; Larkin, A. I.; Nagaoka, Spin-orbit interaction and magnetoresistance in the two dimensional random system. *Y. Progress of Theoretical Physics* **1980**, *63*, (2), 707-710.